Balkan Med J 2026;43:267-280

Overexpression of Circ_0004496 is Associated with Pathological Bone Formation in Ankylosing Spondylitis via the miR-145/ACTG1 Axis

Yu-Cong Zou[1,2], Yong-Sheng Wu[3], Ting Hu[4], Hao-Bin Zeng[3]

[1]Department of Rehabilitation, Zhuhai Hospital of Integrated Traditional Chinese and Western Medicine, Zhuhai, China
[2]Foshan University Affiliated Foshan Fifth People's Hospital, Foshan, China
[3]Department of Orthopedic, Zhuhai Hospital, Guangdong Provincial Hospital of Traditional Chinese Medicine, Zhuhai, China
[4]General Administration of Customs (Beijing) International Travel Health Care Center, Beijing, China

Background: The functional role of circular ribonucleic acids in ankylosing spondylitis (AS) remains poorly understood. In our previous study, circ_0004496 and actin gamma 1 (ACTG1) were found to be upregulated in ossified tissues from patients with AS.

Aims: To investiagate the regulatory role of circ_0004496 in pathological bone formation through the miR-145/ACTG1 axis.

Study Design: Combined *in vitro* and *in vivo* experimental study.

Methods: Tissue samples were obtained from 15 patients with AS and hip ankylosis and 15 control patients with femoral neck fractures. Quantitative real-time polymerase chain reaction was performed to measure circ_0004496 and miR-145 expression. Western blot analysis was used to determine the protein levels of alkaline phosphatase (ALP), osteocalcin (OCN), runt-related transcription factor 2 (Runx2), and ACTG1. Cell proliferation was evaluated using Cell Counting Kit-8 and 5-ethynyl-2′-deoxyuridine assays. Osteogenic differentiation was assessed by measuring ALP activity and performing Alizarin Red S staining. Interactions among circ_0004496, miR-145, and ACTG1 were examined using RNA immunoprecipitation (RIP), RNA pull-down, dual-luciferase reporter, and fluorescence *in situ* hybridization (FISH) assays.

Results: Circ_0004496 and ACTG1 expression levels were significantly elevated in AS hip capsule tissues, whereas miR-145 expression was reduced. Overexpression of circ_0004496 in AS-derived fibroblasts enhanced cell proliferation, accelerated cell cycle progression, increased calcium deposition, and upregulated ALP, OCN, and Runx2 protein levels. Mechanistically, circ_0004496 functioned as a molecular sponge for miR-145, which directly targets ACTG1. These regulatory interactions were confirmed by dual-luciferase reporter, RIP, RNA pulldown, and FISH assays. *In vivo*, circ_0004496 overexpression was associated with sacroiliac joint fusion in proteoglycan-induced arthritis mice.

Conclusion: Circ_0004496 overexpression promotes pathological bone formation in AS by regulating the miR-145/ACTG1 axis both *in vitro* and *in vivo*.

INTRODUCTION

The global incidence of ankylosing spondylitis (AS) is estimated at approximately 2–5%, with substantial disease burden and morbidity.[1] The pathogenesis of AS is characterized by persistent inflammation and pathological new bone formation. Progressive ossification in the sacroiliac joints, spine, and hips frequently results in joint fusion and severe functional impairment.[2] Therefore, preventing aberrant ossification remains a major therapeutic objective in AS management. However, the molecular mechanisms linking chronic inflammation to pathological bone formation are not fully understood. Recent studies have highlighted the involvement of circular RNAs (circRNAs) in various diseases, including AS.[3-6] CircRNAs are single-stranded RNA molecules with a covalently closed circular structure, lacking both 5′ caps and polyadenylated tails. This configuration confers resistance to exonuclease-mediated degradation and contributes to their remarkable stability.[7] Many circRNAs contain multiple microRNA (miRNA)-binding sites.[8] Increasing evidence indicates that specific circRNAs regulate osteogenesis by modulating miRNA activity.[9] For example, circRNA_33287 promotes osteogenic differentiation of maxillary sinus membrane–derived stem cells through the miR-214-3p/Runx3 pathway.[10] CircRNA_0006393 enhances osteogenesis in glucocorticoid-induced osteoporosis by regulating miR-145-5p,[11] whereas circRNA_3626 facilitates skeletal formation via the miR-338-3p/runt-related transcription factor 2 (Runx2) axis.[12] Despite these

Corresponding author: Hao-Bin Zeng, Department of Orthopedic, Zhuhai Hospital, Guangdong Provincial Hospital of Traditional Chinese Medicine, Zhuhai, China
e-mail: Drzenghb@163.com

Received: December 26, 2025 **Accepted:** February 26, 2026 **Available Online Date:** 30.04.2026 • **DOI:** 10.4274/balkanmedj.galenos.2026.2025-12-249
Available at www.balkanmedicaljournal.org

ORCID iDs of the authors: Y.C.Z. 0000-0001-8678-2012; Y.S.W. 0009-0007-6532-3491; T.H. 0009-0000-8233-0166; H.B.Z. 0009-0002-4440-5360.

Cite this article as: Zou YC, Wu YS, Hu T, Zeng HB. Overexpression of Circ_0004496 is Associated with Pathological Bone Formation in Ankylosing Spondylitis via the miR-145/ACTG1 Axis. Balkan Med J. 2026;43:267-280

advances, the roles of circRNAs in AS–particularly in pathological ossification–remain largely unexplored.

miRNAs are short non-coding RNAs that regulate gene expression at the post-transcriptional level by binding to the 3′untranslated regions of target mRNAs, thereby inhibiting translation or promoting mRNA degradation.[13] Through modulation of transcription factors and cytokine signaling pathways, miRNAs influence diverse biological processes.[14] Accumulating evidence implicates specific miRNAs in the pathogenesis of autoimmune diseases, including AS.[15] For instance, miR-96 promotes osteoblast differentiation and bone formation in AS models by activating the Wnt signaling pathway through suppression of suppression of sclerostin.[16] miR-214-3p inhibits osteogenic differentiation of fibroblasts (FBs) derived from AS tissue by blocking the bone morphogenetic protein–transforming growth factor β signaling pathway,[17] and miR-17-5p regulates ectopic bone formation in AS by targeting ankylosis progressive homolog.[18]

MiR-145 is an evolutionarily conserved and widely expressed miRNA encoded by a bicistronic gene cluster.[19] It targets multiple transcription factors, including Krüppel-like factor 4,[20] ELK1 (a member of the ETS transcription factor family),[21] and actin gamma 1 (ACTG1),[22] thereby regulating diverse cellular processes. Notably, miR-145 has been reported to suppress osteogenesis while promoting osteoclastogenesis. It enhances osteoclast formation and exacerbates periarticular bone loss in collagen-induced arthritis by directly inhibiting osteoprotegerin.[23] Furthermore, miR-145 impairs osteogenic differentiation of adipose-derived stem cells by downregulating semaphorin 3A and Sp7,[24,25] and it inhibits chondrogenesis of synovial mesenchymal stem cells (MSCs) through repression of TLR4.[26]

Among the six mammalian actin isoforms, ACTG1 (γ-actin) and ACTB (β-actin) constitute the non-muscle cytoplasmic actin pair essential for maintaining cytoskeletal integrity.[27,28] ACTG1 has been implicated in several pathological conditions, including autosomal dominant hearing loss.[29,30] It also modulates cancer cell behavior[31,32] and contributes to intervertebral disc degeneration through regulation of the NF-κB p65 and Akt signaling pathways.[33] However, the role of ACTG1 in AS has not yet been elucidated.

In our previous bioinformatics analysis,[34] ACTG1 was identified as a potential regulator of abnormal bone formation in AS. Based on this finding, the present study aimed to investigate whether the circ_0004496/miR-145/ACTG1 axis regulates pathological ossification in AS.

MATERIALS AND METHODS

Study patients

Between January 2025 and December 2025, hip capsule tissues were collected from 15 male patients with AS undergoing total hip arthroplasty and 15 male control patients undergoing hip surgery for femoral neck fractures (FNFs) at our hospital. AS was diagnosed according to the Assessment of SpondyloArthritis International Society criteria in combination with the modified New York criteria.[35,36] The mean age was 40.7 ± 3.6 years in the AS group and 42.6 ± 3.4 years in the control group. The study protocol was approved by the Zhuhai Hospital of Integrated Traditional Chinese and Western Medicine Ethics Committee (approval number: 2025-03-023-F01, date: 13.05.2025), and written informed consent was obtained from all human participants.

Tissue collection and fibroblast culture

AS-FBs were isolated from hip capsule tissues as previously described.[37] Tissue samples were minced into fragments approximately 0.5 mm^3 in size, thoroughly rinsed with phosphate-buffered saline (PBS), and digested with collagenase (Sigma-Aldrich, St. Louis, MO, USA). The resulting cell suspensions were filtered through 70-μm cell strainers (BD Biosciences, Franklin Lakes, NJ, USA) to remove debris. Cells were cultured in Dulbecco's Modified Eagle Medium (DMEM; Invitrogen, Carlsbad, CA, USA) supplemented with 10% fetal bovine serum and 1% penicillin–streptomycin. Cultures were maintained at 37 °C in a humidified incubator with 5% CO_2. After initial adhesion, residual tissue fragments were removed, and the culture medium was replaced every 3 days. Cells at passage 3 were used for subsequent experiments.

Quantitative real-time polymerase chain reaction (qRT-PCR) and RNase R assay

Total RNA was extracted using TRIzol reagent (Invitrogen). Complementary DNA (cDNA) was synthesized using the HiScript® II Reverse Transcription Kit (Vazyme, Nanjing, China) for mRNA analysis or the miRNA First Strand cDNA Synthesis Kit (Vazyme) for miRNA detection, employing random primers or oligo$(dT)_{18}$ as appropriate. RNA integrity was assessed using the Agilent 2100 Bioanalyzer with an RNA Nano chip. Only samples with an RNA integrity number ≥7.0 were included in subsequent analyses. To eliminate genomic DNA (gDNA) contamination, purified RNA was treated with RQ1 RNase-free DNase I (Promega, Cat. No. M6101). qRT-PCR was performed using SYBR Premix DimerEraser (Takara, Dalian, China). Relative gene expression levels were calculated using the $2^{-\Delta\Delta Ct}$ method and normalized to glyceraldehyde-3-phosphate dehydrogenase (GAPDH) and U6 as internal reference genes. The primer sequences were as follows: for hsa_circ_0004496, forward 5′-CTGTGTCCAGTGTAGATGAA-3′ and reverse 5′-GCCTGTTCTCTGTTATGTTG-3′; for miR-145, forward 5′-GTCCAGTTTTCCCAGGAA-3′and reverse 5′-CAGGTCAAAAGGGTCCTT-3′; for ACTG1, forward 5′-ATGGAAGGAAACACGGCTC-3′ and reverse 5′-CACTCTGTTCTTCCGCCG-3′; and for U6, forward 5′-CTCGCTTC-GGCAGCACA-3′ and reverse 5′-AACGCTTCACGAATTTGCGT-3′. Primer performance was validated using five cDNA templates prepared in a 10-fold serial dilution to generate standard curves. Amplification efficiencies ranged from 90% to 110%, with correlation coefficients (R^2) greater than 0.99. Melting curve analysis demonstrated a single sharp peak for each amplification product, confirming specificity. Each qPCR plate included a no-template control (NTC) in which cDNA was replaced with nuclease-free water. In all experiments, NTC wells showed Ct values greater than 35 or no amplification signal, excluding false-positive results caused by contamination or primer-dimer formation. To ensure reliable normalization, the stability of GAPDH and U6 expression across AS and FNF samples was evaluated

using the geNorm algorithm. The combination of GAPDH and U6 exhibited high stability (M value < 0.5); therefore, their geometric mean was used as the normalization factor. For RNase R treatment, total RNA was incubated with RNase R (Epicenter, Madison, WI, USA) to confirm the circular structure of circ_0004496.

Western blot analysis

A total of 50 µg of protein was loaded per lane. Protein lysates were prepared from hip capsule tissues and FBs using RIPA lysis buffer (Beyotime, Shanghai, China), followed by separation via 10% SDS-polyacrylamide gel electrophoresis and transfer onto polyvinylidene fluoride membranes. Membranes were blocked with 5% non-fat milk for 2 hours and incubated overnight at 4 °C with primary antibodies, followed by 2 hours of exposure to horseradish peroxidase (HRP)-conjugated secondary antibodies. Protein signals were visualized using enhanced chemiluminescence reagents (Beyotime). Bands were quantified using Image-Pro Plus v6.0 (Silver Spring, MD, USA), and protein levels were normalized to GAPDH. The exposure time was 1 minute for GAPDH and 5 minutes for other proteins. The following antibodies were used: ACTG1 (ab123034, Abcam, 1:1000), Cyclin D1 (ab226977, Abcam, 1:1000), c-Myc (ab152146, Abcam, 1:1000), osteocalcin (OCN; ab93876, Abcam, 1:1000), alkaline phosphatase (ALP; ab224335, Abcam, 1:1000), Runx2 (ab23981, Abcam, 1:800), GAPDH (ab9485, Abcam, 1:2000), and HRP-conjugated secondary antibody (ab205718, Abcam, 1:1000), all obtained from Abcam (Cambridge, MA, USA).

Subcellular fractionation

Cytoplasmic and nuclear RNA fractions were isolated using the PARIS kit (Ambion, Austin, TX, USA) according to the manufacturer's instructions. U6 and 18S rRNA were used as nuclear and cytoplasmic markers, respectively.

Cell transfection

The lentiviral vector for circ_0004496 overexpression (OE-circ_0004496) and the control lentiviral vector were synthesized by Genechem Biotechnology (Shanghai, China). Lentivirus transfection was performed at a multiplicity of infection (MOI) of 50, achieving approximately 80% transfection efficiency in rat FBs. At 48 hours postinfection, green fluorescent protein expression was observed under a fluorescence microscope to confirm successful transfection.

miR-145 mimic was synthesized by Ribobio (Guangzhou, China) and transfected into cells using Lipofectamine™ 3000 (L3000015, Invitrogen™), following the manufacturer's protocol.

Flow cytometry for cell cycle analysis

Cell cycle analysis was performed using a gating strategy in which cell population gates were defined in FSC-A vs. SSC-A scatter plots to exclude debris, followed by single-cell gating in FSC-H vs. FSC-A plots to exclude aggregates. Single cells were then analyzed using PI-A (fluorescence intensity) histograms. Before fixation, trypan blue staining confirmed that cell viability was > 95%. After fixation with 70% ethanol and PI staining (Vazyme), debris and dead cells were excluded by FSC/SSC gating. Cells were incubated in binding buffer and labeled with propidium iodide for 20 minutes at room temperature. The cell cycle distribution was subsequently assessed using a flow cytometer (BD Biosciences).

5′-Ethynyl-2′-deoxyuridine (EdU) incorporation assay

Cell proliferation was evaluated using an EdU detection kit (Ribobio, Guangzhou, China) following the manufacturer's instructions. Transfected FBs were plated in 24-well plates and exposed to EdU solution. After incubation, cells were fixed with paraformaldehyde and permeabilized with 0.5% Triton X-100. EdU incorporation was visualized via fluorescent staining, and nuclei were counterstained with DAPI. Fluorescent images were captured using an Olympus microscope (Tokyo, Japan). The percentage of EdU-positive nuclei was quantified.

ALP activity assay

ALP activity was measured using a colorimetric assay kit (Nanjing Jiancheng Bioengineering Institute, China) according to the manufacturer's protocol.

Alizarin red staining

Osteogenic differentiation was assessed 10 days post-transfection under osteogenic conditions. The osteogenic medium consisted of DMEM-LG supplemented with 20% fetal calf serum, 10 mL/L penicillin–streptomycin (5 IU/mL), 1% non-essential amino acids, 2.5 mg/L amphotericin B (250 µg/mL), 50 µg/mL L-ascorbic acid 2-phosphate, 100 nM dexamethasone, and 10 mM β-glycerophosphate. Cells were stained with 40 mM Alizarin Red solution (pH 4.2; Sigma-Aldrich, Shanghai, China) for 30 minutes, washed thoroughly, and air-dried. Calcified nodules were photographed, and the stain was extracted using 10% cetylpyridinium chloride. Absorbance was measured at 510 nm, and dye quantification was performed using a calibration curve.

RNA fluorescence in situ hybridization (FISH)

Fluorescent probes targeting circ_0004496 (Cy3-labeled) and miR-145 (FITC-labeled) were custom-synthesized by Geneseed Biotechnology (Guangzhou, China). AS FBs were seeded on coverslips, fixed, permeabilized, and dehydrated. Hybridization was performed overnight at 37 °C. After hybridization, cells were washed thoroughly, stained with DAPI (4′,6-diamidino-2-phenylindole) to visualize nuclei, and mounted for imaging. Images were captured using a Leica TCS SP2 AOBS confocal microscope (Germany).

RNA immunoprecipitation (RIP) assay

RIP was performed using the Magna RIP™ Kit (Millipore, Bedford, MA, USA). FBs were lysed and incubated with magnetic beads conjugated to anti-IgG or anti-Ago2 antibodies. The abundance of circ_0004496, ACTG1, and miR-145 was quantified from the immunoprecipitated RNA.

RNA pull-down assay

Biotin-labeled wild-type (WT) and mutant (MUT) miR-145, along with negative control oligonucleotides (bio-NC), were purchased from Sangon (Shanghai, China) and transfected into AS FBs. RNA complexes were isolated using streptavidin-conjugated magnetic beads (Invitrogen), and the levels of circ_0004496 and ACTG1 were quantified by qRT-PCR.

Dual luciferase reporter assay

Sequences from circ_0004496 and the 3′ untranslated region (3′-UTR) of ACTG1 containing miR-145 target sites were cloned into the pmirGLO vector (Promega, Fitchburg, WI, USA) to generate WT and MUT constructs. Plasmids were cotransfected with miR-145 mimics or controls into AS FBs. Luciferase activity was measured using the Dual-Luciferase Reporter Assay System (Promega).

Proteoglycan-induced AS mouse model

Eight-month-old female BALB/c mice, weighing approximately 24 ± 2 g, were obtained from Guangzhou Chase Reward Co. Ltd, China. Mice were housed under specific pathogen-free conditions on a 12-hour light/dark cycle with ad libitum access to food and water. The AS model was established as previously described by intraperitoneal injection of 200 µL of emulsion (100 µg cartilage proteoglycan + 100 µL PBS + 100 µL complete Freund's adjuvant) on days 0, 21, and 42.[38] Mice were anesthetized with 3% sevoflurane and euthanized via cervical dislocation. All procedures were approved by the Zhuhai Hospital of Integrated Traditional Chinese and Western Medicine Animal Experiment Committee (approval number. 2025-0011, dated: 13.05.2025) and were conducted in accordance with institutional guidelines.

Circ_0004496 overexpression in vivo

To evaluate the effect of circ_0004496 *in vivo*, proteoglycan-induced arthritis (PGIA) mice were randomly assigned at week 16 into three groups (n = 6 per group): control vector or circ_0004496 overexpression vector. Mice were numbered for identification, and the researcher performing histological analyses was blinded to group allocation. Constructs were synthesized by Genscript (Shanghai, China) and delivered via tail vein injection (2 mg/kg) for systemic expression.

Histological analysis

At 24 weeks, mice were humanely sacrificed, and sacroiliac joint tissues were harvested. Tissues were fixed in 4% paraformaldehyde, decalcified in EDTA for 4 weeks, dehydrated in ethanol, and embedded in paraffin. Sections were generated and stained with hematoxylin and eosin for microscopic histopathological analysis.

Statistical analysis

Statistical analyses were performed using GraphPad Prism v10.0. Data normality was assessed using the Shapiro-Wilk test. Normally distributed data were compared using the unpaired two-tailed Student's t-test for two-group comparisons or one-way ANOVA followed by Bonferroni correction for comparisons among multiple groups. Pearson's correlation coefficient was used to evaluate associations. Cell experiments were performed in three independent runs (cell line or single-donor experiments). p values < 0.05 were considered statistically significant.

RESULTS

Elevated expression of circ_0004496 and ACTG1 in hip capsule tissues from patients with AS

The demographic characteristics of the AS and FNF groups are summarized in Tables 1 and 2. To evaluate the expression of circ_0004496, miR-145, and ACTG1 mRNA in hip capsule tissues, qRT-PCR assays were performed. AS samples exhibited significantly higher levels of circ_0004496 (Figure 1a) and ACTG1 mRNA (Figure 1c), and low level of miR-145 (Figure 1b). Spearman's correlation analysis further revealed a positive correlation between ACTG1 and circ_0004496 levels, whereas circ_0004496 levels were inversely correlated with miR-145 levels in AS tissues (Figure 1d, e).

To confirm these results at the protein level, Western blotting was performed to assess ACTG1 and key osteogenic markers, including ALP, Runx2, and OCN. Compared with the FNF group, the AS group showed significantly increased expression of ACTG1, ALP, Runx2, and OCN (Figure 1f, g), suggesting enhanced osteogenic activity and a role for ACTG1 in AS-associated pathological bone formation.

TABLE 1. Characteristic of Patients with Ankylosing Spondylitis.

No.	1	2	3	4	5	6	7	8	9	10	11	12	13	14	15
Diagnosis	AS	AS	AS	AS	AS	AS	AS	AS	AS	AS	AS	AS	AS	AS	AS
Age (y)	44	38	41	47	39	40	35	41	42	48	38	41	40	36	40
Sex (f/m)	M	M	M	M	M	M	M	M	M	M	M	M	M	M	M
BMI (kg/m^2)	22.1	21.8	19.5	20.3	20.1	18.6	21.2	17.9	19.1	18.5	20.6	19.3	21.3	17.8	18.8
Duration of disease (y)	7.3	8.2	6.9	9.2	6.5	8.8	10.3	7.5	8.0	7.6	9.2	7.5	8.3	7.9	7.7
HLA-B27	+	+	+	+	+	+	+	+	+	+	+	+	+	+	+
BASDAI	4.2	3.9	4.9	5.3	5.6	5.0	5.2	4.9	4.6	4.8	5.2	5.5	5.4	4.5	4.9
NSAIDS used	Yes	Yes	Yes	Yes	Yes	Yes	Yes	Yes	Yes	Yes	Yes	Yes	Yes	Yes	Yes
TNF-α inhibitor used	Yes	Yes	Yes	Yes	no	Yes	no	Yes	Yes	Yes	Yes	Yes	Yes	Yes	Yes
mSASSS score	44	43	50	55	52	49	60	57	38	45	47	42	55	54	49
NY Grade	4	4	4	4	4	4	4	4	4	4	4	4	4	4	4
ID	AS01	AS02	AS03	AS04	AS05	AS06	AS07	AS08	AS09	AS10	AS11	AS12	AS13	AS14	AS15

BASDAI, bath ankylosing spondylitis disease activity index; NSAIDS, non-steroidal anti-inflammatory drugs, TNF-α, tumor necrosis factor alpha; mSASSS score, modified stoke ankylosing spondylitis spine score; f/m, female/male.

TABLE 2. Characteristic of Patients with Femoral Neck Fracture.

No.	1	2	3	4	5	6	7	8	9	10	11	12	13	14	15
Diagnosis	FNF	FNF	FNF	FNF	FNF	FNF	FNF	FNF	FNF	FNF	FNF	FNF	FNF	FNF	FNF
Age (y)	45	40	39	43	37	49	41	44	47	40	43	44	38	46	43
Sex (f/m)	M	M	M	M	M	M	M	M	M	M	M	M	M	M	M
BMI (kg/m^2)	21.6	23.8	21.8	22.5	23.1	22.0	21.0	18.5	20.1	19.2	20.4	18.9	21.3	20.5	17.8

BMI, body mass index; f/m, female/male.

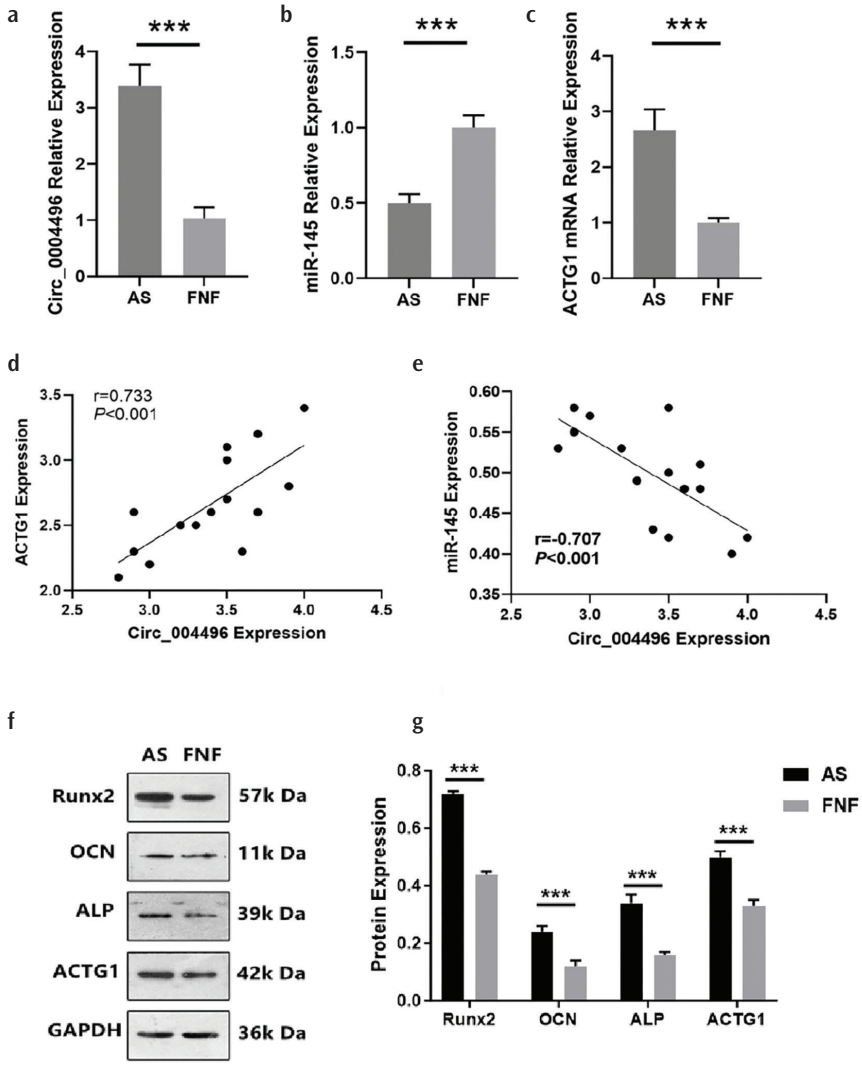

FIG. 1. Circ_0004496, miR-145, and ACTG1 mRNA expression levels in the hip capsule tissues from the AS and FNF groups were quantified via qRT-PCR. (a) Circ_0004496 was significantly upregulated in AS compared with FNF, while (b) miR-145 was downregulated. (c) ACTG1 expression was markedly increased in AS relative to FNF (n = 15, ***$p < 0.001$ vs. FNF). (d) ACTG1 levels were found to be positively associated with circ_0004496 levels, while (e) miR-145 levels were negatively correlated with circ_0004496 levels in AS hip capsule tissues. (f) Representative western blot bands of Runx2, ALP, OCN, and ACTG1 are shown, with (g) quantitative analysis revealing significantly higher expression of these osteogenesis-related proteins in the AS group compared to the FNF group. AS, ankylosing spondylitis; FNF, femoral neck fracture; ACTG1, actin gamma 1; Runx2, runt-related transcription factor 2; ALP, alkaline phosphatase; OCN, osteocalcin; qRT-PCR, quantitative real-time polymerase chain reaction.

Characteristics of circ_0004496

Circ_0004496 is located on chromosome 4 (chr4:177632653–177650900) and originates from exons 2–4 of the vascular endothelial growth factor C *(VEGFC)* gene (Figure 2a). Using divergent primers, a specific amplification product of circ_0004496 was detected exclusively in cDNA from AS FBs, but not in gDNA (Figure 2b), confirming its circular structure. Resistance to RNase R digestion further supported this, as circ_0004496 remained stable while the linear control gene GAPDH was degraded (Figure 2c). Subcellular fractionation analysis revealed that circ_0004496 is predominantly localized in the cytoplasm of AS FBs (Figure 2d), indicating cytoplasmic enrichment and structural stability.

Osteogenic potential assessed by flow cytometry and WB analysis

Cells from both groups were successfully cultured (Figure 3a, b). To assess osteogenic potential, flow cytometry and Western blotting analyses were performed. Flow cytometry was initially used to analyze the cellular composition of AS and FNF groups. The proportion of $CD105^+$ and $CD90^+$ cells in patients with AS was higher than in patients with FNF (Figure 3c, d), suggesting an enrichment of MSC-like populations in AS FBs. Additionally, $CD34^-$ and $CD45^-$ cells were identified in AS and FNF groups (Figure 3e, f).

Circ_0004496 promoted proliferation and cell cycle progression in AS FBs (AS05)

To explore the role of circ_0004496 in AS FBs, a lentiviral vector for circ_0004496 overexpression was constructed and transfected into AS FBs alongside a control vector. The MOI was 50, achieving an 80% transfection rate. Cell proliferation was assessed using EdU and Cell Counting Kit-8 assays. These analyses indicated that circ_0004496 overexpression markedly enhanced FB proliferation (Figure 4a-c). In contrast, transfection with a miR-145 mimic significantly reduced cell viability, proliferation, and cell cycle progression.

Flow cytometry analysis further revealed that circ_0004496 overexpression promoted S-phase entry and reduced the proportion of cells in the G0/G1 phase (Figure 4d, e). Conversely, the miR-145 mimic suppressed S-phase progression and increased the G0/G1 population. Western blotting confirmed that circ_0004496 overexpression upregulated Cyclin D1, a key cell cycle regulator, and c-Myc, a proliferation-associated protein, in AS FBs.

Circ_0004496 overexpression promoted osteogenic differentiation of AS FBs (AS05)

Next, we examined the effect of circ_0004496 on the osteogenic differentiation of AS FBs. Overexpression of circ_0004496 significantly increased calcium deposition and ALP activity. It also elevated the expression of key osteogenic markers, including ALP, OCN, and Runx2. Conversely, miR-145 overexpression attenuated these effects, suggesting that circ_0004496 enhances osteogenic

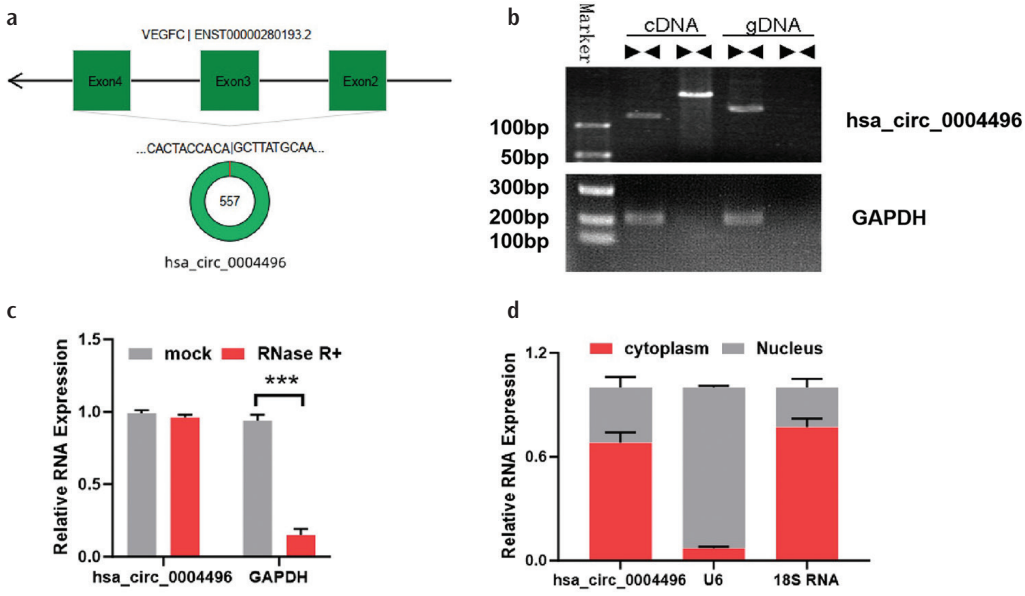

FIG. 2. Characteristics of circ_0004496. (a) Circ_0004496 originates from the *VEGFC* gene. (b) Divergent primers specifically amplified circ_0004496 in cDNA from AS FBs, but no amplification was observed in genomic DNA (gDNA), confirming its circular structure. (c) Total RNA extracted from FBs derived from AS was subjected to RNase R treatment or left untreated. The levels of circ_0004496 and GAPDH were quantified by qRT-PCR. Circ_0004496 demonstrated greater resistance to RNase R -mediated degradation relative to GAPDH. (d) The subcellular localization of circ_0004496 in FBs derived from AS was determined via qRT-PCR, revealing that circ_0004496 is predominantly expressed in the cytoplasm. ***$p < 0.001$. AS, ankylosing spondylitis; gDNA, genomic DNA; FB, fibroblasts; cDNA, complementary DNA; qRT-PCR, quantitative real-time polymerase chain reaction.

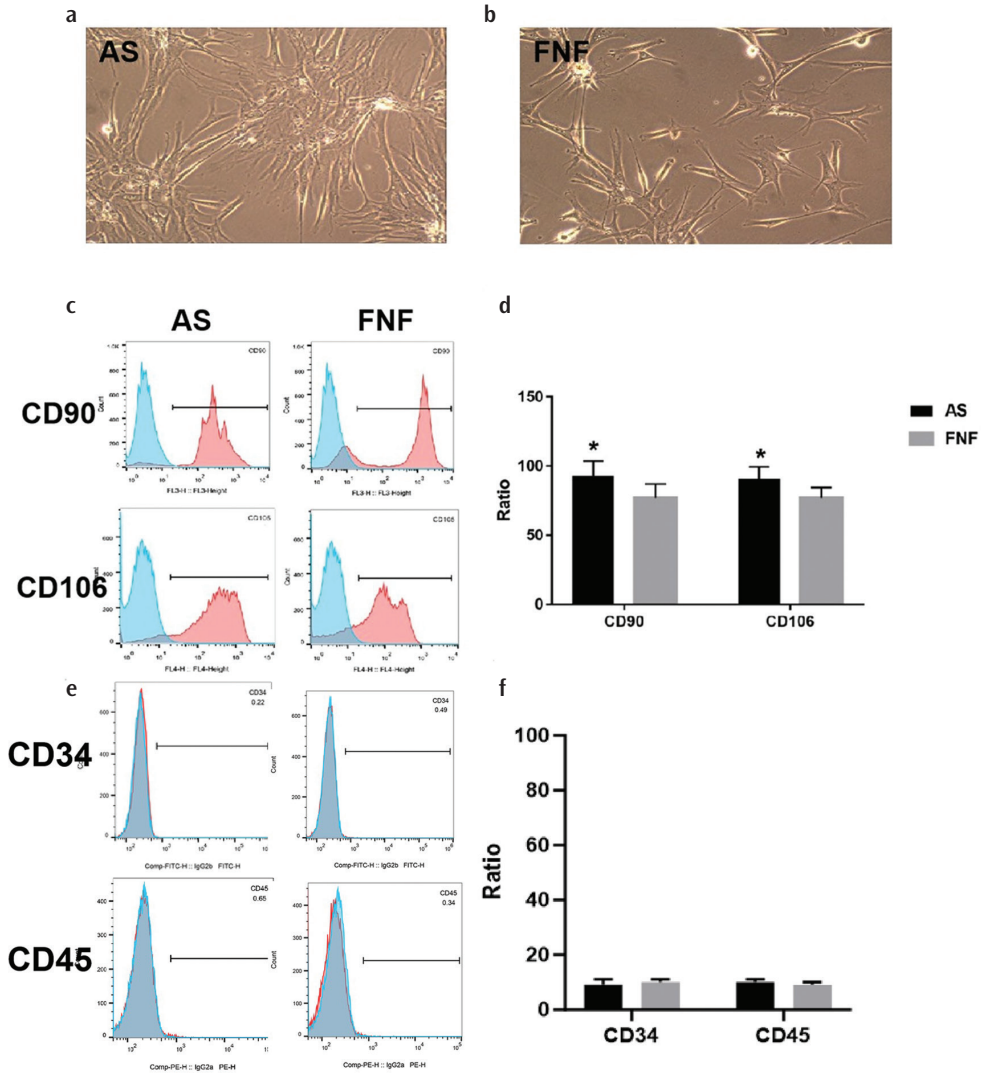

FIG. 3. Osteogenic differentiation determined by flow cytometry and western blot analysis. (a) Primary cultured cells from the AS group. (b) Primary cultured cells from the FNF group. (c) Representative flow cytometry plots showing CD90 and CD105 expression in AS and FNF groups. (d) Ratio of CD90 and CD105 positive cells between AS and FNF groups. (e) Representative flow cytometry plots showing CD34 and CD45 expression in AS and FNF groups. (f) Ratio of CD34 and CD45 positive cells between AS and FNF groups. AS, ankylosing spondylitis; FNF, femoral neck fracture.

potential in AS FBs, whereas miR-145 acts as a negative regulator (Figure 5a-c, Figure 6a, b). Collectively, these results indicate that circ_0004496 facilitates osteogenic differentiation in FBs derived from AS tissues.

We also evaluated the osteogenic potential of ACTG1 in AS FBs using Alizarin Red S staining and ALP activity assays. Recombinant ACTG1 protein (Cat. No. ab157841, Abcam) was applied to upregulate ACTG1 expression, whereas an anti-ACTG1 antibody (Cat. No. A8481, Sigma-Aldrich) was used to knock down ACTG1. ACTG1 overexpression markedly enhanced calcium deposition and ALP activity, whereas ACTG1 inhibition significantly reduced both measures (Figure 7a-c).

Circ_0004496 regulates ACTG1 expression by targeting miR-145

CircRNAs can function as molecular sponges for miRNAs, thereby modulating the expression of target genes. To determine whether circ_0004496 regulates ACTG1 via miRNA interaction, bioinformatic analyses were performed using StarBase (http://starbase.sysu.edu.cn/) together with and circInteractome (https://circinteractome.irp.nia.nih.gov/). These analyses identified miR-145 as having binding sites in circ_0004496 and the 3′-UTR of ACTG1 (Figure 8a, b).

Dual-luciferase reporter assays (DLRA) showed that miR-145 overexpression significantly reduced the luciferase activity of WT circ_0004496 and ACTG1 3′-UTR constructs, whereas MUT constructs with disrupted miR-145 binding sites were unaffected in AS FBs) (Figure 8c, d).

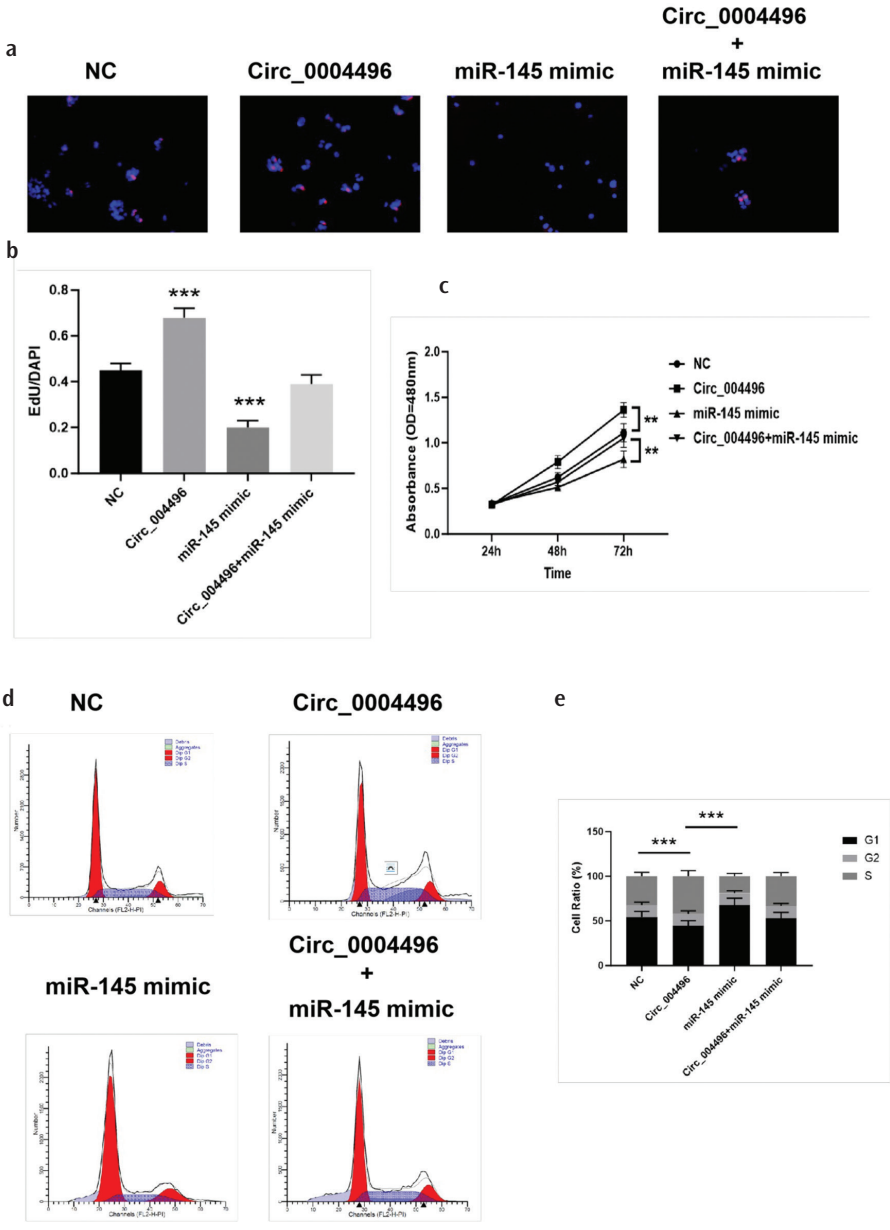

FIG. 4. Overexpression of circ_0004496 enhances proliferation and osteogenic differentiation in AS FBs. AS FBs were transfected with circ_0004496 and miR-145 mimics. (a) Cell proliferation was assessed via EdU incorporation assay, and circ_0004496 expression levels were measured by qRT-PCR. (b) Quantification analysis of EdU-positive cells. (c) Cell viability was evaluated using the CCK-8 assay (Statistical significance was determined by two-way Repeated Measures analysis of variance with Bonferroni's post test.$^{**}p < 0.01$ vs. control). (d) Cell cycle distribution was determined by flow cytometry. (e) Statistical analysis of cell cycle phase proportions. $^{**}p < 0.01$, $^{***}p < 0.001$. AS, ankylosing spondylitis; FB, Fibroblasts; ALP, alkaline phosphatase; qRT-PCR, quantitative real-time polymerase chain reaction.

FISH further confirmed the interaction between circ_0004496 and miR-145, revealing their colocalization in AS FBs (Figure 9a). RIP assays demonstrated significant enrichment of circ_0004496, ACTG1, and miR-145 in anti-AGO2 immunoprecipitates compared with IgG controls (Figure 9b). Additionally, RNA pull-down assays indicated that biotinylated WT miR-145 (WT-bio-miR-145) markedly enriched circ_0004496 and ACTG1 RNA relative to negative control (bio-NC) or miR-145 (MUT-bio-miR-145) probes (Figure 9c). Collectively, these results indicate that circ_0004496 promotes ACTG1 expression by sponging miR-145.

AS FBs were visualized with green for miR-145, red for circ_0004496, blue for DAPI, and yellow indicating signal overlap. Scale bar, 20 μm. RIP assays showed the association between miR-145 and circ_0004496/ACTG1, with summarized results representing relative expression in AS FBs after different treatments ($^{***}p < 0.001$ vs. anti-IgG). RNA pull-down assays demonstrated the association between miR-145 and circ_0004496/ACTG1 ($^{***}p < 0.01$ vs. bio-NC) RIP; FB, FBs.

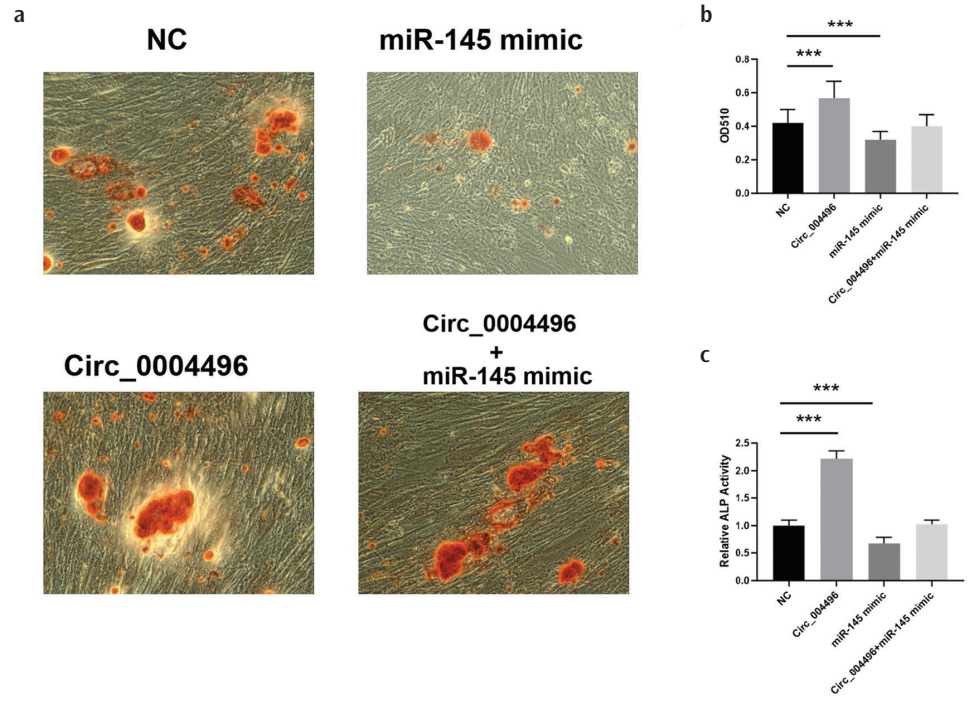

FIG. 5. Calcification nodules formed in AS FBs across different groups. FBs were cultured and transfected with specified plasmids for 10 days, followed by ARS. For quantification, Alizarin red was eluted with cetylpyridinium chloride (10%). Optical density was measured at the wavelength of 510 nm. (a) Representative images of Alizarin red staining. (b) The activity of ossification was quantified by ARS staining (***$p < 0.001$ vs. NC). (c) Quantification of ALP activity (***$p < 0.001$ vs. NC). ARS, Alizarin Red S; FBs, fibroblasts; AS, ankylosing spondylitis; ALP, alkaline phosphatase.

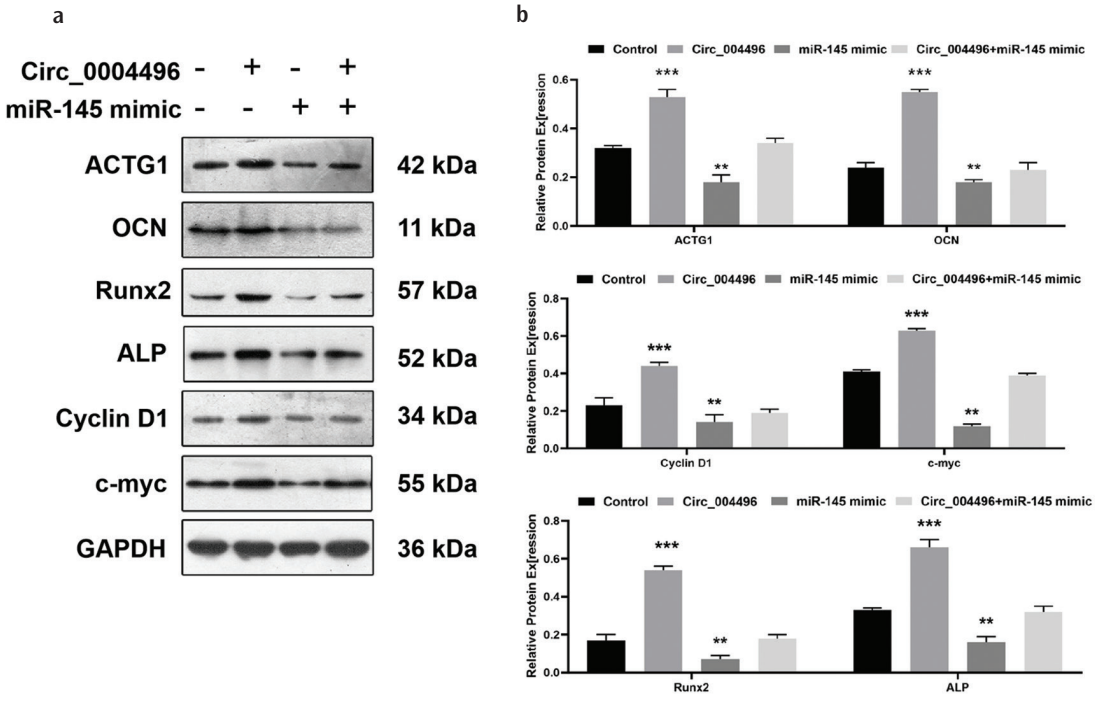

FIG. 6. (a) Protein expression of ACTG1, osteogenesis-related markers (OCN, Runx2, ALP), and cell cycle-related markers (Cyclin D1, c-Myc). (b) Quantitative analysis of protein expression following circ_0004496 overexpression or miR-145 mimic intervention. **$p < 0.001$ vs. control ***$p < 0.01$ vs. control. ACTG1, actin gamma 1; ALP, alkaline phosphatase; Runx2, runt-related transcription factor 2; OCN, osteocalcin.

Circ_0004496 overexpression is associated with sacroiliac joint fusion in PGIA mice

To evaluate the role of circ_0004496 in AS-associated ankylosis, mice received either a circ_0004496 overexpression vector or a control vector via tail vein injection. Overexpression of circ_0004496 significantly promoted sacroiliac joint fusion compared with the control group (circ_0004496: 75% ± 5% vs. control: 10% ± 0.5%, $p < 0.001$; Figure 10), indicating a pathological role for circ_0004496 in AS progression *in vivo*.

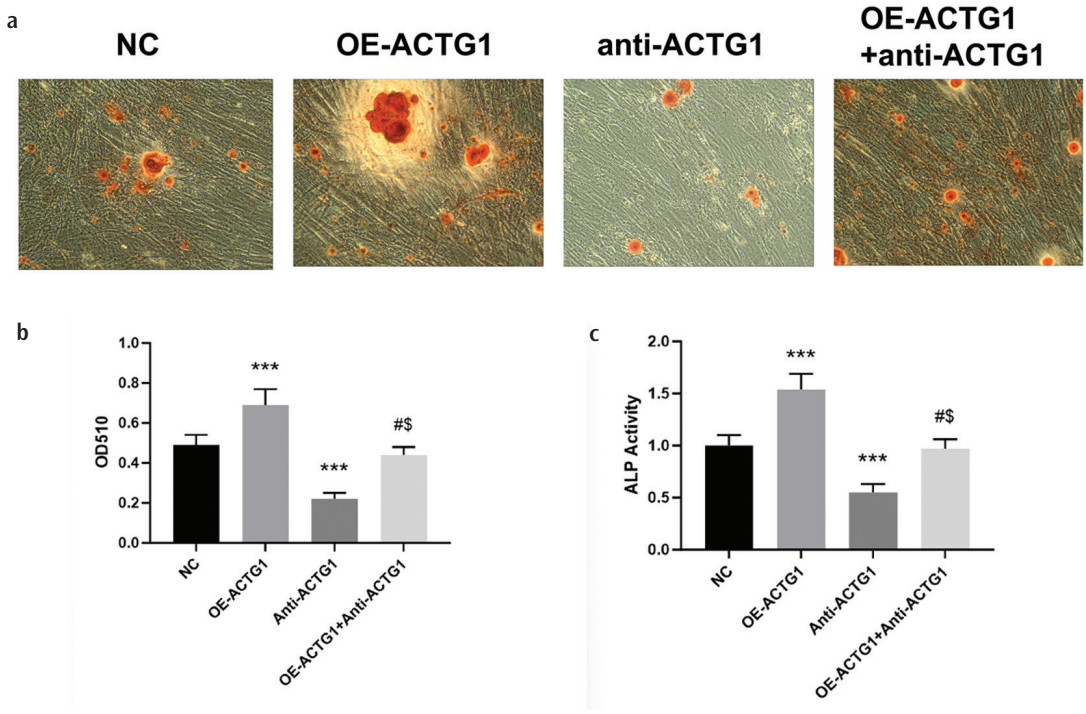

FIG. 7. Calcification nodules formed in AS FBs across following ACTG1 overexpression or anti-ACTG1 internention. Optical density was measured at the wavelength of 510 nm. (a) Representative images of Alizarin red staining. (b) The activity of ossification was quantified by ARS staining (***$p < 0.001$ vs. NC). (c) Quantification of ALP activity (***$p < 0.001$ vs. NC). $^{\#}p < 0.05$ vs. ACTG1 overexpression group; $^{\$}p<0.05$ vs. anti- ACTG1 group. ARS, Alizarin Red S; FBs, fibroblasts; AS, ankylosing spondylitis; ACTG1, actin gamma 1.

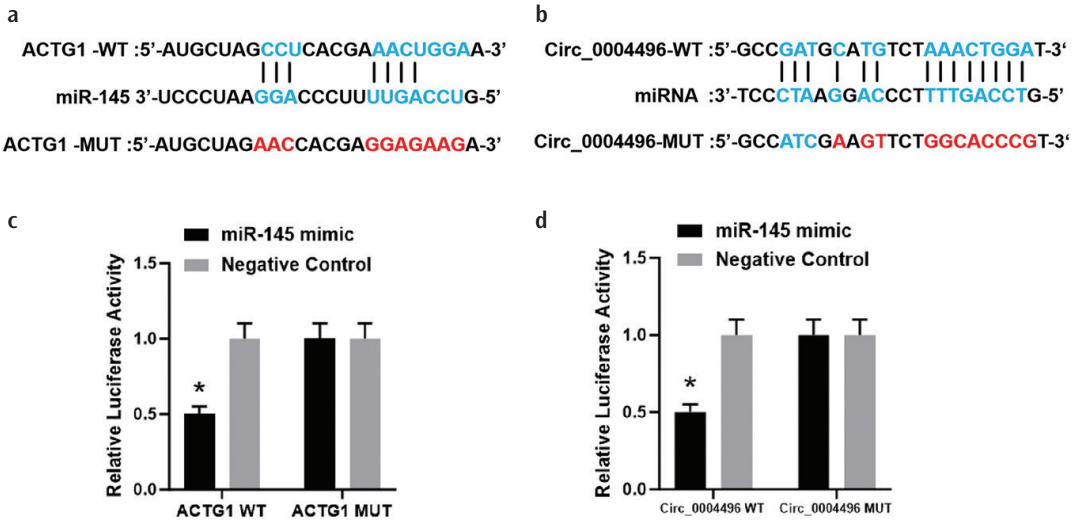

FIG. 8. (a, b) Potential miR-145 binding sites on circ_0004496 and ACTG1 were predicted using the Starbase and CircInteractome databases. (c, d) Dual-luciferase reporter assays were performed in AS FBs co-transfected with either miR-NC or miR-145, alongside WT or MUT constructs of circ_0004496 and ACTG1 3′-UTR. WT, wild-type; MUT, mutant; FBs, fibroblasts; ACTG1, actin gamma 1.

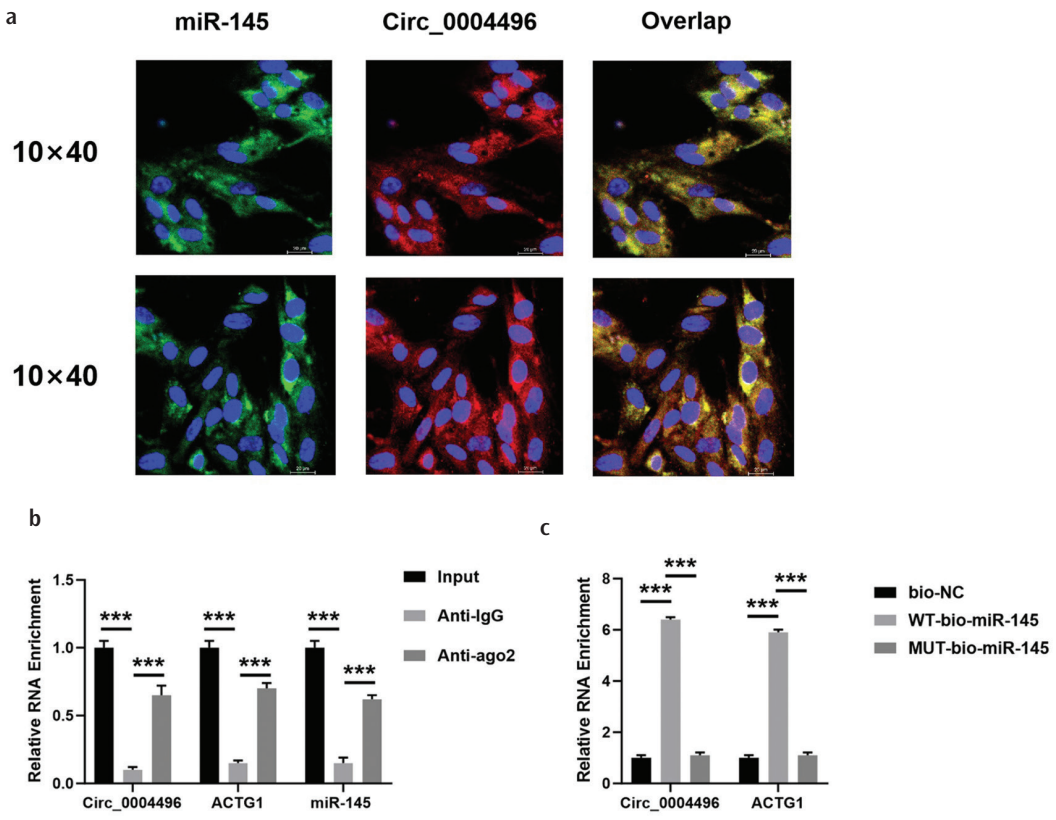

FIG. 9. (a) Representative images showing the localization of circ_0004496 and microRNA-145 in AS FBs [green: miR-145; red: circ_0004496; blue: 4',6-diamidino-2-phenylindole (DAPI); yellow: overlap of signals]. Scale bar: 20 μm. (b) RIP assay showing association between miR-145 and circ_0004496/ACTG1. Summarized results show relative expression of miR-145 and circ_0004496 in AS FBs after different treatments (***$p < 0.001$ vs. anti-IgG). (c) RNA pull-down assay showing association between miR-145 and circ_0004496/ACTG1. ***$p < 0.01$ vs. bio-NC. RIP, RNA immunoprecipitation; FBs, fibroblasts.

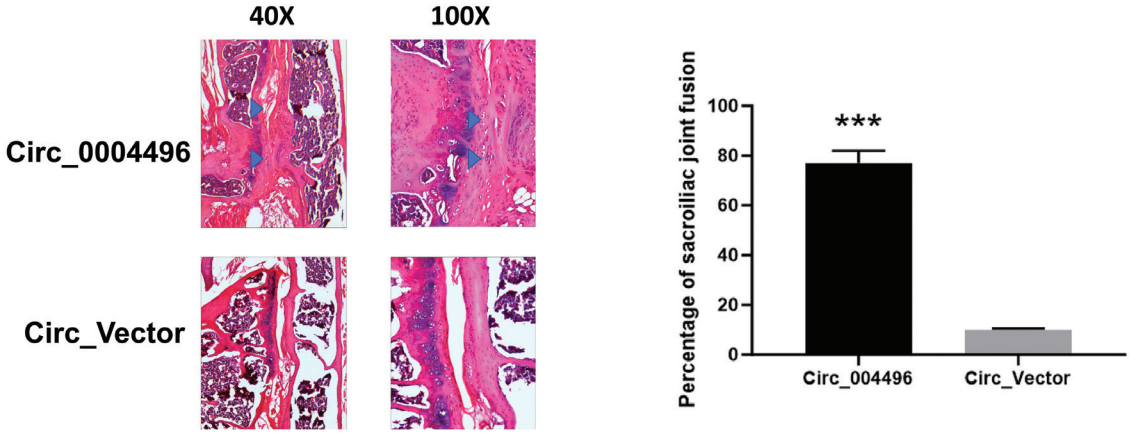

FIG. 10. Tail vein injection of circ_0004496 overexpression vector induced sacroiliac joint fusion in PGIA mice compared with control vector.

DISCUSSION

In this study, we demonstrated that both circ_0004496 and ACTG1 were significantly upregulated in hip capsule specimens from patients with AS, whereas miR-145 expression was markedly downregulated. Overexpression of circ_0004496 in AS FBs promoted cell proliferation, accelerated cell cycle progression, and enhanced calcium deposition, accompanied by increased protein levels of ALP, OCN, and Runx2. Mechanistically, circ_0004496 acted as a molecular sponge for miR-145, which directly targets ACTG1. This regulatory axis was validated using a combination of DLRA, RIP, RNA pull-down, and FISH. Furthermore, *in vivo* overexpression of circ_0004496 in PGIA mice was associated with sacroiliac joint fusion, underscoring its pathological role in AS-related abnormal bone formation via the miR-145/ACTG1 axis.

Currently, only a few circRNAs have been implicated in AS pathogenesis. For example, circ_0056558 suppresses cellular activity in AS by downregulating miR-1290 and upregulating CDK6.[39] Circ_0018168 inhibits FB proliferation and osteogenic differentiation by sponging miR-330-3p, thereby increasing DKK1 expression.[40] Additionally, circIFNGR2 modulates AS-related inflammation by regulating macrophage polarization.[41] Our study adds circ_0004496, derived from the *VEGFC* gene, to this growing list of functionally relevant circRNAs (Figure 2).

Enthesitis and bone erosion are hallmarks of early AS and are characterized by inflammation at ligament, tendon, or joint capsule attachment sites. These tissues are relatively avascular but are surrounded by lymphatic vessels.[42] Injury to these regions triggers an inflammatory response that promotes lymphangiogenesis.[43] Notably, tendon injury has been associated with a pronounced increase in lymphatic vessel formation,[44-46] although the underlying molecular mechanisms remain incompletely understood. Prior studies have shown that tendon injury combined with systemic trauma induces lymphatic vessel infiltration into adjacent tissues, a process correlated with elevated VEGFC levels.[47] This suggests that VEGFC may serve as a key mediator linking tissue injury and pathological ossification, implicating circ_0004496 as a potential contributor to the transition from AS-associated bone erosion to abnormal new bone formation.

MiR-145 has been reported to suppress chondrogenesis and bone formation, including osteogenic differentiation, osteoblastogenesis, and bone regeneration, by regulating Wnt signaling and other pathways involved in bone homeostasis.[48-50] Conversely, miR-145 promotes osteoclastogenesis, thereby exacerbating bone erosion.[51] In AS, a reduction in miR-145 levels during the initial 3 months of anti-TNF treatment may reflect a transition from early bone erosion to reparative processes, as evidenced by subsequent new bone formation.[52]

Our previous bioinformatics analysis predicted that ACTG1 is prominently expressed within the focal adhesion and Rap1 signaling pathways in AS.[34] Consistent with this prediction, the present study confirmed significant upregulation of ACTG1 in AS hip tissues. ACTG1 encodes cytoplasmic actin γ1, a ubiquitously expressed cytoskeletal protein critical for cell motility and structural integrity. Elevated ACTG1 expression has been linked to extracellular matrix receptor interactions and is implicated in human chondrocyte apoptosis.[53-55] Shimohira et al.[56] demonstrated that YAG laser bone ablation modulates BCAR1 and ACTG1 expression, key regulators of mechanotransduction and bone healing. Similarly, Li et al.[57] showed that in osteoarthritis, chondrocytes increased the levels of COL6A3 and ACTG1, thereby promoting the transformation of FBs via activation of the focal adhesion pathway. Furthermore, KEGG and GO analyses by Liu et al.[58] connected ACTG1 to immune-related cellular functions in RA. Collectively, these findings support a role for ACTG1 in bone remodeling during advanced stages of AS through focal adhesion and Rap1 signaling.

Several limitations of this study should be considered. Firstly, the sample size was relatively small, with 15 patients per group in the clinical study and 6 animals per group in the animal study. On the one hand, the number of AS patients developing hip ankylosis is comparatively low. On the other hand, some patients with AS are unwilling to undergo surgery. Thus, larger cohorts are needed to validate these findings. The cohort size for the clinical study was determined by sample availability, while the number of animals followed common practice in pilot *in vivo* studies in the field. Secondly, although the circ_0004496/miR-145/ACTG1 axis was preliminarily validated, the downstream signaling pathways of ACTG1 in osteogenic differentiation (e.g., Rap1, focal adhesion) remain unexplored. Thirdly, the expression of CD90 and CD105 suggests a potential MSC-like phenotype within the FB population. Differences in marker expression between AS and control groups indicate inherent variations in cell populations that could influence osteogenic potential. We present this observation as part of the phenotypic characterization of AS-derived cells rather than as a confounding factor, and it may contribute to the observed functional differences. Further experiments, including quantitative PCR and Western blotting, are required to clarify these effects. Fourthly, we did not account for medical confounding factors, such as the dose or duration of TNF inhibitor or NSAID use by patients. Fifthly, only overexpression of circ_0004496 was investigated in cell experiments. Additional knockdown assays are necessary to provide more robust evidence of the pathogenic role of circ_0004496 in AS bone formation. Finally, we did not measure VEGFC or lymphatic markers, despite identifying circ_0004496 as originating from VEGFC. Further studies are warranted to investigate VEGFC/lymphangiogenesis in abnormal bone formation in AS.

In summary, our preliminary study demonstrated that overexpression of circ_0004496 is associated with pathological bone formation in AS through regulation of the miR-145/ACTG1 axis. These findings provide new insights into the molecular mechanisms underlying AS progression and highlight potential therapeutic targets of circRNAs.

Ethics Committee Approval: The study protocol was approved by the Zhuhai Hospital of Integrated Traditional Chinese and Western Medicine Ethics Committee (approval number: 2025-03-023-F01, date: 13.05.2025) and all procedures were approved by the Zhuhai Hospital of Integrated Traditional Chinese and Western Medicine Animal Experiment Committee (approval number: 2025-0011, dated: 13.05.2025).

Informed Consent: Written informed consent was obtained from all human participants.

Data Sharing Statement: The data that support the findings of this study are available from the corresponding author upon reasonable request.

Authorship Contributions: Concept- Y.C.Z.; Design- Y.C.Z., Y.S.W.; Funding- Y.C.Z.; Data Collection or Processing- T.H.; Analysis and/or Interpretation- T.H.; Writing- Y.C.Z., H.B.Z.; Critical Review- H.B.Z.

Conflict of Interest: The authors declare that they have no conflict of interest.

Funding: This work was supported by the Guangdong Basic and Applied Basic Research Foundation (No. 2022A1515140130), Foshan Health Bureau Project (20230826A010547), the Youth Elite Scientists Sponsorship Program by CACM (No. CACM-2024-QNRC2-A06) and Guangdong provincial scientific research project of traditional Chinese Medicine (No. 20261359).

REFERENCES

1. Wei Y, Zhang S, Shao F, Sun Y. Ankylosing spondylitis: from pathogenesis to therapy. *Int Immunopharmacol*. 2025;145:113709. [CrossRef]
2. Klavdianou K, Kanellou A, Daoussis D. Molecular mechanisms of new bone formation in axial spondyloarthritis. *Mediterr J Rheumatol*. 2022;33:115-125. [CrossRef]
3. Tang YP, Zhang QB, Dai F, et al. Circular RNAs in peripheral blood mononuclear cells from ankylosing spondylitis. *Chin Med J (Engl)*. 2021;134:2573-2582. [CrossRef]
4. Zhang L, Qu L, Zhang Y, Xu Z, Tang H. Differential expression of circular RNAs in plasma exosomes from patients with ankylosing spondylitis. *Cell Biol Int*. 2022;46:649-659. [CrossRef]
5. Fang Y, Liu J. Novel regulatory role of non-coding RNAs in ankylosing spondylitis. *Front Immunol*. 2023;14:1131355. [CrossRef]
6. Abbas AA, Abdulkader HA, Giordo R, et al. Implications and theragnostic potentials of circular RNAs in rheumatic diseases. *Int J Biol Macromol*. 2023;235:123783. [CrossRef]
7. Zhou WY, Cai ZR, Liu J, et al. Circular RNA: metabolism, functions and interactions with proteins. *Mol Cancer*. 2020;19:172. [CrossRef]
8. Kour B, Gupta S, Singh R, Sophiarani Y, Paul P. Interplay between circular RNA, microRNA, and human diseases. *Mol Genet Genomics*. 2022;297:277-286. [CrossRef]
9. Huang W, Wu Y, Qiao M, et al. CircRNA-miRNA networks in regulating bone disease. *J Cell Physiol*. 2022;237:1225-1244. [CrossRef]
10. Peng W, Zhu S, Chen J, et al. Hsa_circRNA_33287 promotes the osteogenic differentiation of maxillary sinus membrane stem cells via miR-214-3p/Runx3. *Biomed Pharmacother*. 2019;109:1709-1717. [CrossRef]
11. Wang XB, Li PB, Guo SF, et al. circRNA_0006393 promotes osteogenesis in glucocorticoid induced osteoporosis by sponging miR 145 5p and upregulating FOXO1. *Mol Med Rep*. 2019;20:2851-2858. [CrossRef]
12. Chen G, Wang S, Wei R, et al. Circular RNA circ-3626 promotes bone formation by modulating the miR-338-3p/Runx2 axis. *Joint Bone Spine*. 2024;91:105669. [CrossRef]
13. Ho PTB, Clark IM, Le LTT. MicroRNA-based diagnosis and therapy. *Int J Mol Sci*. 2022;23:7167. [CrossRef]
14. Saliminejad K, Khorram Khorshid HR, Soleymani Fard S, Ghaffari SH. An overview of microRNAs: biology, functions, therapeutics, and analysis methods. *J Cell Physiol*. 2019;234:5451-5465. [CrossRef]
15. Liu C, Yang H, Shi W, Wang T, Ruan Q. MicroRNA-mediated regulation of T helper type 17/regulatory T-cell balance in autoimmune disease. *Immunology*. 2018;155:427-434. [CrossRef]
16. Ma S, Wang DD, Ma CY, Zhang YD. microRNA-96 promotes osteoblast differentiation and bone formation in ankylosing spondylitis mice through activating the Wnt signaling pathway by binding to SOST. *J Cell Biochem*. 2019;120:15429-15442. [CrossRef]
17. Ding L, Yin Y, Hou Y, et al. microRNA-214-3p suppresses ankylosing spondylitis fibroblast osteogenesis via BMP-TGFβ axis and BMP2. *Front Endocrinol (Lausanne)*. 2021;11:609753. [CrossRef]
18. Qin X, Zhu B, Jiang T, et al. miR-17-5p regulates heterotopic ossification by targeting ANKH in ankylosing spondylitis. *Mol Ther Nucleic Acids*. 2019;18:696-707. [CrossRef]
19. Zeinali T, Mansoori B, Mohammadi A, Baradaran B. Regulatory mechanisms of miR-145 expression and the importance of its function in cancer metastasis. *Biomed Pharmacother*. 2019;109:195-207. [CrossRef]
20. Sun W, Zhou S, Peng L, et al. CircZNF609 regulates pulmonary fibrosis via miR-145-5p/KLF4 axis and its translation function. *Cell Mol Biol Lett*. 2023;28:105. [CrossRef]
21. Nazari M, Ni NC, Lüdke A, et al. Mast cells promote proliferation and migration and inhibit differentiation of mesenchymal stem cells through PDGF. *J Mol Cell Cardiol*. 2016;94:32-42. [CrossRef]
22. Ren L, Wang L, Yi X, et al. Ultrasound microbubble-stimulated miR-145-5p inhibits malignant behaviors of breast cancer cells by targeting ACTG1. *Ultrasound Q*. 2024;40:136-143. [CrossRef]
23. Chen Y, Wang X, Yang M, et al. miR-145-5p increases osteoclast numbers in vitro and aggravates bone erosion in collagen-induced arthritis by targeting osteoprotegerin. *Med Sci Monit*. 2018;24:5292-5300. [CrossRef]
24. Liu X, Zhu W, Wang L, et al. miR-145-5p suppresses osteogenic differentiation of adipose-derived stem cells by targeting semaphorin 3A. *In Vitro Cell Dev Biol Anim*. 2019;55:189-202. [CrossRef]
25. Jia J, Tian Q, Ling S, et al. miR-145 suppresses osteogenic differentiation by targeting Sp7. *FEBS Lett*. 2013;587:3027-3031. [CrossRef]
26. Wu M, Liu F, Yan L, et al. MiR-145-5p restrains chondrogenic differentiation of synovium-derived mesenchymal stem cells by suppressing TLR4. *Nucleosides Nucleotides Nucleic Acids*. 2022;41:625-642. [CrossRef]
27. Rubenstein PA. The functional importance of multiple actin isoforms. *Bioessays*. 1990;12:309-315. [CrossRef]
28. Sundby LJ, Southern WM, Hawbaker KM, et al. Nucleotide- and protein-dependent functions of Actg1. *Mol Biol Cell*. 2022;33:ar77. [CrossRef]
29. van Wijk E, Krieger E, Kemperman MH, et al. A mutation in the gamma actin 1 (ACTG1) gene causes autosomal dominant hearing loss (DFNA20/26). *J Med Genet*. 2003;40:879-884. [CrossRef]
30. Kemerley A, Sloan C, Pfeifer W, Smith R, Drack A. A novel mutation in ACTG1 causing Baraitser-Winter syndrome with extremely variable expressivity in three generations. *Ophthalmic Genet*. 2017;38:152-156. [CrossRef]
31. Xiao L, Peng H, Yan M, Chen S. Silencing ACTG1 expression induces prostate cancer epithelial mesenchymal transition through MAPK/ERK signaling pathway. *DNA Cell Biol*. 2021;40:1445-1455. [CrossRef]
32. Chen S, Wang X, Yuan J, et al. Reduced levels of actin gamma 1 predict poor prognosis in ovarian cancer patients. *J Obstet Gynaecol Res*. 2020;46:1827-1834. [CrossRef]
33. Wu T, Jia X, Feng H, Wu D. ACTG1 regulates intervertebral disc degeneration via the NF-κB-p65 and Akt pathways. *Biochem Biophys Res Commun*. 2021;545:54-61. [CrossRef]
34. Zou YC, Wu J, Zhao C, Luo ZR. Analysis of circular RNA expression profile of pathological bone formation in ankylosing spondylitis. *Int J Rheum Dis*. 2023;26:1403-1406. [CrossRef]
35. Rudwaleit M, van der Heijde D, Landewé R, et al. The development of Assessment of SpondyloArthritis international Society classification criteria for axial spondyloarthritis (part II): validation and final selection. *Ann Rheum Dis*. 2009;68:777-783. Erratum in: *Ann Rheum Dis*. 2019;78:e59. [CrossRef]
36. van der Heijde D, Baraliakos X, Sieper J, et al. Efficacy and safety of upadacitinib for active ankylosing spondylitis refractory to biological therapy: a double-blind, randomised, placebo-controlled phase 3 trial. *Ann Rheum Dis*. 2022;81:1515-1523. [CrossRef]
37. Zou YC, Yang XW, Yuan SG, et al. Downregulation of dickkopf-1 enhances the proliferation and osteogenic potential of fibroblasts isolated from ankylosing spondylitis patients via the Wnt/β-catenin signaling pathway in vitro. *Connect Tissue Res*. 2016;57:200-211[CrossRef]
38. Zou YC, Yan LM, Gao YP, Wang ZY, Liu G. miR-21 may Act as a potential mediator between inflammation and abnormal bone formation in ankylosing spondylitis based on TNF-α concentration-dependent manner through the JAK2/STAT3 pathway. *Dose Response*. 2020;18:1559325819901239. [CrossRef]
39. Li X, Zhou W, Li Z, Guan F. Hsa_circ_0056558 regulates cyclin-dependent kinase 6 by sponging microRNA-1290 to suppress the proliferation and differentiation in ankylosing spondylitis. *Autoimmunity*. 2021;54:114-128. [CrossRef]
40. Zhao L, Jiao J, Yan G, et al. Circ_0018168 inhibits the proliferation and osteogenic differentiation of fibroblasts in ankylosing spondylitis via regulating miR-330-3p/DKK1 axis. *Regen Ther*. 2022;21:175-184. [CrossRef]
41. Song M, Wang X, Gao J, et al. circIFNGR2 regulating ankylosing spondylitis-associated inflammation through macrophage polarization. *iScience*. 2023;26:107325. [CrossRef]
42. Edwards DA. The blood supply and lymphatic drainage of tendons. *J Anat*. 1946;80:147-152.2. [CrossRef]
43. Abouelkheir GR, Upchurch BD, Rutkowski JM. Lymphangiogenesis: fuel, smoke, or extinguisher of inflammation's fire? *Exp Biol Med (Maywood)*. 2017;242:884-895. [CrossRef]

44. Tong X, Zhang T, Li S, et al. Rotator cuff healing is regulated by the lymphatic vasculature. *J Orthop Translat*. 2022;38:65-75. [CrossRef]
45. Tempfer H, Kaser-Eichberger A, Korntner S, et al. Presence of lymphatics in a rat tendon lesion model. *Histochem Cell Biol*. 2015;143:411-419. [CrossRef]
46. Tempfer H, Traweger A. Tendon vasculature in health and disease. *Front Physiol*. 2015;6:330. [CrossRef]
47. Vishlaghi N, Guo L, Griswold-Wheeler D, et al. Vegfc-expressing cells form heterotopic bone after musculoskeletal injury. *Cell Rep*. 2024;43:114049. [CrossRef]
48. Jia J, Tian Q, Ling S, et al. miR-145 suppresses osteogenic differentiation by targeting Sp7. *FEBS Lett*. 2013;587:3027-3031. [CrossRef]
49. Yang B, Guo H, Zhang Y, et al. MicroRNA-145 regulates chondrogenic differentiation of mesenchymal stem cells by targeting Sox9. *PLoS One*. 2011;6:e21679. [CrossRef]
50. Hao W, Liu H, Zhou L, et al. MiR-145 regulates osteogenic differentiation of human adipose-derived mesenchymal stem cells through targeting FoxO1. *Exp Biol Med (Maywood)*. 2018;243:386-393. [CrossRef]
51. Fukuda T, Ochi H, Sunamura S, et al. MicroRNA-145 regulates osteoblastic differentiation by targeting the transcription factor Cbfb. *FEBS Lett*. 2015;589:3302-3308. [CrossRef]
52. Chen Y, Wang X, Yang M, et al. miR-145-5p increases osteoclast numbers in vitro and aggravates bone erosion in collagen-induced arthritis by targeting osteoprotegerin. *Med Sci Monit*. 2018;24:5292-5300. [CrossRef]
53. Bunnell TM, Burbach BJ, Shimizu Y, Ervasti JM. β-Actin specifically controls cell growth, migration, and the G-actin pool. *Mol Biol Cell*. 2011;22:4047-4058. [CrossRef]
54. Shum MS, Pasquier E, Po'uha ST, et al. γ-Actin regulates cell migration and modulates the ROCK signaling pathway. *FASEB J*. 2011;25:4423-4433. [CrossRef]
55. Tsolis KC, Bei ES, Papathanasiou I, et al. Comparative proteomic analysis of hypertrophic chondrocytes in osteoarthritis. *Clin Proteomics*. 2015;12:12. [CrossRef]
56. Shimohira T, Katagiri S, Ohsugi Y, et al. Comprehensive and sequential gene expression analysis of bone healing process following er:YAG laser ablation. *Photobiomodul Photomed Laser Surg*. 2021;39:100-112. [CrossRef]
57. Li C, Luo J, Xu X, et al. Single cell sequencing revealed the underlying pathogenesis of the development of osteoarthritis. *Gene*. 2020;757:144939. [CrossRef]
58. Liu J, Chen N. A 9 mRNAs-based diagnostic signature for rheumatoid arthritis by integrating bioinformatic analysis and machine-learning. *J Orthop Surg Res*. 2021;16:44. [CrossRef]